ADVANCED SUSTAINABLE SYSTEMS
www.advsustainsys.com

Experimental Characterization of a Novel Fluidized-Bed Zn–Air Fuel Cell

Alessio Mattia Gesualdo, Marco Milanese, Gianpiero Colangelo, and Arturo de Risi*

Zn–air fuel cells are promising energy storage devices for renewable energy and power sources, as they are cost-effective and have high energy density. However, limited charge and discharge cycles and low round-trip efficiency have long been obstacles to large-scale market deployment. Herein, a new fluidized-bed zinc–air fuel cell is designed, constructed, tested, and characterized. The integration of the fluidized bed in the zinc–air fuel cell leads to key advantages such as: erosion of the anode passivation layer, which plays a key role in the rapid voltage decay and keeping the products of reactions away from the proximity of the electrodes, reducing the concentration overpotential, due to the concentration gradient of electrode species in the diffusion boundary layer between the electrode–electrolyte interface and the electrolyte bulk.

1. Introduction

Over the last few decades, the phenomenon of pollution and global warming, mainly due to energy production plants and vehicles, has become increasingly evident. This issue highlighted the importance of reducing emissions through renewable and sustainable energy sources, such as solar or wind, coupled with energy storage systems.[1,2] Nowadays, renewable energy is widely adopted in many countries to rebalance energy portfolio and reduce environmental impact of greenhouse gas emissions.[3] Furthermore, the recent Russia–Ukraine war has made the transition to renewable energy even more urgent because of rising fossil energy prices.

However, energy storage is a crucial factor in making renewable sources completely reliable as fossil sources. Essentially, renewable energy should be stored in case of excess in production and then released, during low generation period. Energy storage systems constitute therefore an integral and indispensable part of a reliable and effective renewable and distributed generation unit.[4] Hence, the increasing deployment of energy storage systems can offer technical and environmental advantages, such as: power quality improvement, mitigation of voltage deviation, frequency regulation, load shifting, load levelling and peak shaving, facilitation of renewable energy source integration, network expansion and overall cost reduction, operating reserves, and greenhouse gases reduction.[5] Energy storage devices must have high efficiency, large storage capacity, high specific power, and must be inexpensive.

The extraordinary environmental quality and high efficiency of fuel cells make them a potential alternative energy source.[1,6–8] A fuel cell is an electrochemical device that directly converts chemical energy of fuel into electricity. The one-step (from chemical to electrical energy) nature of this process, in comparison to the multistep (e.g., from chemical to thermal to mechanical to electrical energy) processes involved in combustion-based engines, offers the benefit to reduce the efficiency losses being each step characterized by its own efficiency and the global efficiency given by the product of the efficiency of all steps. Additionally, fuel cells are compatible with renewable sources. Their inherent modularity allows simple construction for a wide range of applications in portable and stationary power generation. In short, fuel cells provide a cleaner, more efficient and flexible chemical-to-electrical energy conversion system.[7–9]

1.1. Fluidized-Bed Zinc–Air Fuel Cell: State of the Art

In recent years zinc–air batteries and fuel cells received increasing attention because of their high theoretical energy density; moreover, zinc as anode also has other advantages, such as stability in aqueous alkaline electrolytes, low cost, low toxicity, easy, and safe storage and handling.[10–12]

Compared to the hydrogen proton exchange membrane fuel cell, the catalysts of zinc air fuel cell are made by nonprecious metals such as manganese dioxide;[10] for this reason some researchers focused on the development of air electrodes with high catalyst activity and low costs, such as manganese-based catalysts, on which excellent results have been reached by Sapkota et al.,[13] Ma et al.,[14] Lee et al.,[15] and Sumboja et al.;[12] besides, other researchers focused on N-doped carbon nanotubes catalytic materials[16–18] and nanoporous carbon nanofiber films.[19]

A. M. Gesualdo, M. Milanese, G. Colangelo, A. de Risi
Department of Engineering for Innovation
University of Salento
Lecce 73100, Italy
E-mail: marco.milanese@unisalento.it

The ORCID identification number(s) for the author(s) of this article can be found under https://doi.org/10.1002/adsu.202300103

DOI: 10.1002/adsu.202300103

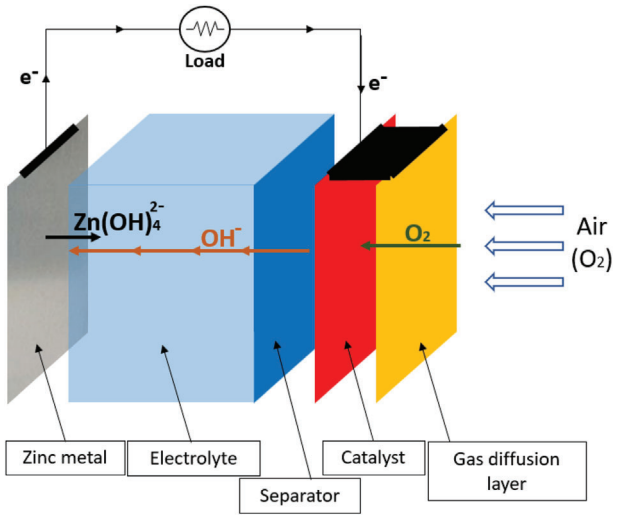

Figure 1. Composition and principle of operation of a zinc–air electrochemical device.

A typical zinc–air fuel cell (ZAFC) is composed of a zinc electrode as an anode, a membrane separator, an air electrode as a cathode (which is divided into a gas diffusion layer and a catalytic active layer) and an alkaline electrolyte, as shown in **Figure 1**. Upon cell discharge, zinc oxidation occurs, giving rise to soluble zincate ions $Zn(OH)_4^{2-}$; this process usually proceeds until they are supersaturated in the electrolyte, after which the zincate ions precipitate as insoluble zinc oxide.[6,8,20]

The overall electrochemical reaction taking place in the ZAFC can be analyzed by considering the anode and cathode reactions separately. Hereafter, the anodic, cathodic, and the overall reaction are shown with their standard equilibrium potentials[6,21,22]

- ANODIC REACTION:

$$Zn + 4OH^- \rightarrow Zn(OH)_4^{2-} + 2e^- \quad (E^0_{a,r} = -0.625\ V)$$
$$Zn(OH)_4^{2-} \rightarrow ZnO + H_2O + 2OH^- \quad (1)$$

- CATHODIC REACTION:

$$O_2 + 4e^- + 2H_2O \rightarrow 4OH^- \quad (E^0_{c,r} = +0.400\ V) \quad (2)$$

- OVERALL REACTION:

$$2Zn + O_2 + H_2O + 2OH^- \rightarrow 2Zn(OH)_4^{2-} \quad (E^0_{eq,r} = 1.65\ V) \quad (3)$$

ZnO is generally considered as the final product of a ZAFC, as long as the reaction occurs in the saturated concentration of zincate. Nevertheless, solid ZnO is an electrical insulator and has higher molar volumes than metallic zinc. Their precipitation on a zinc electrode might cause passivation and gradually decrease the specific capacity of cell. The relevant precipitation rates depend on the alkali concentration (that decreases during discharge) and the applied current density. Hence, ZnO. formation hinders the development of ZAFCs.[21,23,24]

In parallel with the oxidation reaction at the negative electrode, an undesired parasitic reaction between zinc and water can occur, resulting in hydrogen gas generation (hydrogen evolution reaction)[20,24–27]

$$Zn + 2H_2O \rightarrow Zn(OH)_2 + H_{2\,(g)} \quad (4)$$

Moreover, as the cell operates with air instead of pure oxygen, the CO_2 present in the air dissolves in the electrolyte forming carbonate

$$CO_2 + OH^- \rightarrow HCO_3^- \quad (5)$$

$$HCO_3^- + OH^- \leftrightarrow CO_3^{2-} + H_2O \quad (6)$$

The formation of carbonate increases the viscosity of the electrolyte and decreases its ionic conductivity. In a ZAFC, this effect can be minimized by continuously supplying a fresh electrolyte solution.[28,29]

Many research groups proposed different approaches to solve the operating problems of ZAFCs, such as unreacted zinc, solid products, and by-products in the electrolyte. For example, some integrated systems of flowing electrolyte and zinc particles have been proposed. One of these system is the tapered-end structure,[6,30] in which there are two surfaces which are not parallel to each other, with a little vertical angle; this angle produces a difference between the lower and upper ends. A continuous flow of electrolyte is maintained from the top to the bottom of the cell. When the cell starts to discharge, pellets reduce their size due to the chemical reaction and flow on the downside by natural movements. Solid products and by-products as well as small size unreacted zinc particles escape out from the cell along with the effluent of electrolyte. The major disadvantage of this system is the presence of inactive volume in the hopper, which inevitably increases the weight of the cell, reducing its efficiency.[6,28]

The tapered-end solution has been utilized from many research groups, such as Pei et al.,[10] and Han et al.,[31] in order to obtain high performance ZAFCs; the higher performance has been reached by Pei et al.[10] who obtained a peak power density of 435 mW cm^{-2}.

A different solution was proposed by Sangeetha et al.[32] with a fluidized bed ZAFC in which zinc particles were used as anode and KOH solution as flowing electrolyte: through this configuration they improved the performance of the ZAFC. Nevertheless, in their study there was a lack on how determine the optimal flowing rates of the ZAFC, which can be determined by empirical methods or trial-and error methods.[23]

In an integrated system of flowing electrolyte and zinc particles, the following positive impacts can be highlighted

i. Flowing electrolyte through the cell is highly advantageous as this can inhibit hydrogen evolution reaction.[23] In fact, being endothermic this parasitic process, the flow of electrolyte through the cell may reduce the heating up to the level required to mitigate the H_2 generation.
ii. The use of zinc particles provides a greater active surface area than other configurations improving the reactions between zincate and OH^-.
iii. The electrolyte flow field can be designed to erode the anode passivation layer, which plays a key role in swift voltage decay.[22,33]

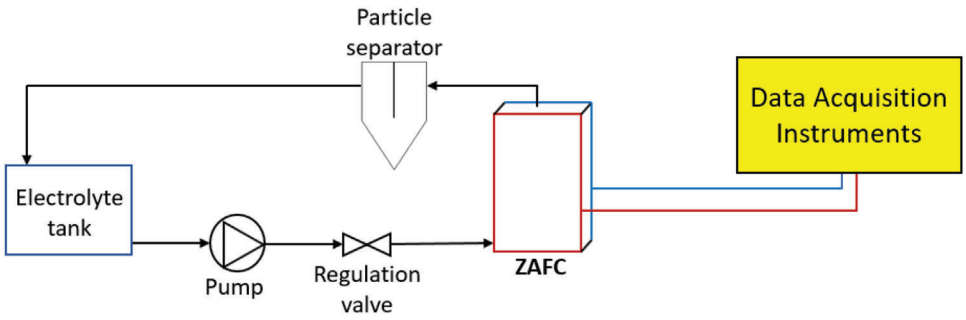

Figure 2. Schematic of the experimental setup.

iv. The ZnO precipitation can be removed from ZAFC by the electrolyte circulation.[22,33]
v. The flow of electrolyte plays an important role in keeping the products of reactions away from the proximity of the electrodes, reducing the concentration overpotential[22,10] (potential difference due to the concentration gradient of the electrode species in the diffusion boundary layer between the electrode–electrolyte interface and the bulk of the electrolyte).
vi. The carbonate precipitation can be rinsed away by the flowing electrolyte.[22]

In the present work, a novel fluidized-bed ZAFC has been designed, built, tested, and characterized, in order to reach a number of key advantages, such as low cost, high theoretical specific energy, high safety characteristic associated with its manufacturing process, storage, and handling, high electrochemical equivalent capacity.[34] Hence, it lends itself well to the various purposes that are required of an energy storage system. Moreover, differently from the above resumed scientific researches, the attention of the present paper was focused also on the fluidization parameters, which allow to obtain an efficient, economical, and reliable electrochemical storage device.

2. Experimental Section

2.1. Air Cathode

A typical ZAFC cathode (air electrode) consists of three layers: a current collecting layer, a gas diffusion layer, and a catalytic active layer.[35] It is reasonable to assume that type and amount of each material and structure of the air electrode affects the ZAFC performance.[24,28,35]

The catalyst is needed to minimize the large activation energy losses related to the oxygen reduction reaction (ORR).[24] Many noble metal catalysts, such as Pt, Ru, and Ir, have been studied to improve the ORR activity, but due to their high cost, a lot of works have focused their attention on alkaline systems, based on transition metal oxides.[24,35–37] Gorlin et al.[38] and Sapkota et al.[28] reported that manganese oxide (MnO_x) showed high activity for both ORR and OER (oxygen evolution reaction), similar to that of noble metal catalysts.[24,35,13]

Hence, in the experimental setup of the present work an economic three-layers air electrode was used; particularly, the catalyst was MnO_2 arranged on a graphitic layer, while the current collecting layer was realized by means of a Nickel mesh and the gas diffusion layer was composed of PTFE.

2.2. Electrolyte

The anode reaction which occurs in alkaline electrolyte allows to have a higher equilibrium potential difference in the cell than in the case of an electrolyte with an acidic or neutral pH value.[29] For this reason, the most used aqueous alkaline electrolyte in zinc–air batteries are those containing potassium hydroxide (KOH), sodium hydroxide (NaOH), and lithium hydroxide (LiOH). Among these, KOH has been extensively used because of the fast electrochemical kinetics, the high solubility of zinc salts and the higher ionic conductivity of K^+ (73.50 Ω^{-1} cm^{2}equiv^{-1}) compared to Na^+ (50.11 Ω^{-1} cm^{2}equiv^{-1}) or Li^+ (38.7 Ω^{-1} cm^{2}equiv^{-1}).[24,39]

In addition to the importance of using an alkaline electrolyte, it is also necessary to choose the right concentration: increasing the concentration of KOH can reduce the resistance of the electrolyte, but too high concentration can lead to increased viscosity[24] and cause faster consumption of the zinc anode.[40] According to the conclusions reached by Thomas et al.[41] and by Sangeetha et al.,[32] in this experimental setup it was chosen a KOH concentration of 40 wt%.

2.3. Separator

The function of the separator in a zinc–air cell is to transport the hydroxyl ions (OH^-) from the air electrode to the electrolyte and at the same time it physically isolates the positive and negative electrodes.[24] The basic requirements of a proper separator are stability in alkaline solution, appropriate pore size and porosity, high ionic conductivity, and electrical nonconductivity.[24] In this work, a PTFE sheet, having the above-cited characteristics, was used as separator.

2.4. Experimental Setup

According to the schematic of **Figure 2**, the experimental setup was composed, in addition to the ZAFC, by: i) a tank from which the electrolyte was pumped into the hydraulic circuit of the ZAFC; ii) three pressure sensors, by which it was possible

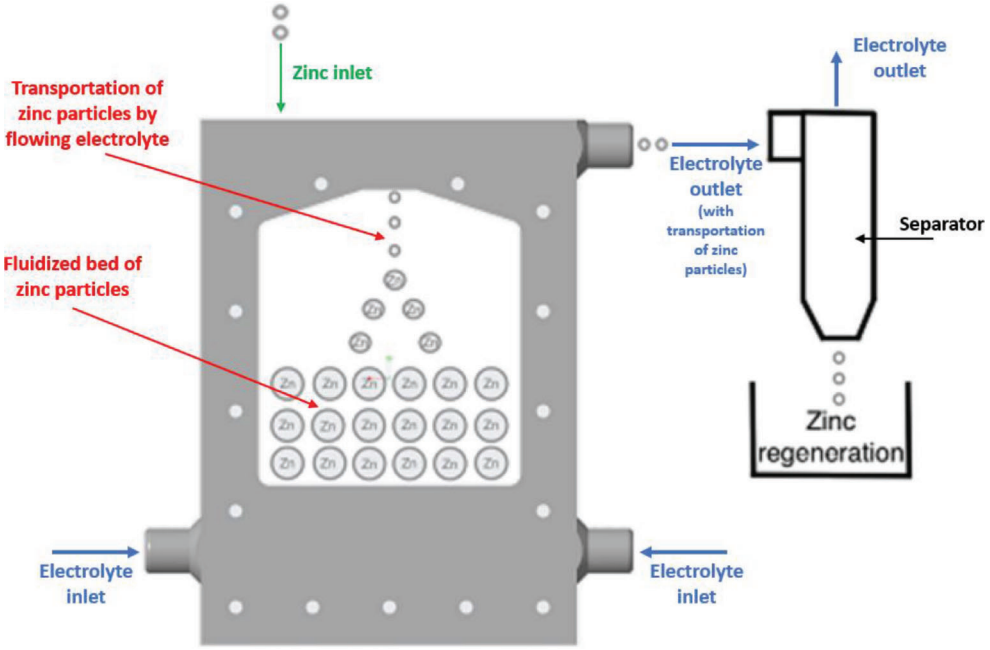

Figure 3. Schematic of the fluidized bed ZAFC.

to monitor the pressure drop of the flux in the hydraulic circuit; iii) a flow meter and a regulating valve, which controlled the flow rate; iv) a separator which allowed the separation of the smallest zinc particles, carried away from the fluid bed, by the electrolyte.

Figure 3 shows the schematic of the fluidized bed ZAFC. The cell is 15 cm high, 10 cm wide, and 2 cm deep; it has two inlet channels by which the flow is homogeneously distributed at the bottom of the fluid bed. **Figure 4** shows an image of the entire experimental setup.

2.5. Experimental Method

The relationship between fluidized bed parameters and ZAFC performance was evaluated in various steps. First, the fluidized bed has been characterized by measuring height of the bed, flow rate of electrolyte and pressures in different points of the setup. As second step, the polarization curves related to different flow rate conditions were analyzed. Finally, the third step was the performance analysis during the operating time. These analyses were conducted in two different fluid dynamic conditions: fixed expanded bed and fluidized bed. In this phase, the energy conversion efficiency, which is defined as the ratio between the actual energy production and the energy which could be produced theoretically from the same amount of zinc, has been calculated, according to the following equation[42,43]

$$\eta_{\text{conversion}} = \frac{W_{\text{el}}}{\Delta G} = \frac{W_{\text{el}}}{-n \cdot F \cdot E_{\text{r}}} \tag{7}$$

where W_{el} is the electrical energy produced by the cell, ΔG is the theoretical Gibbs free energy, n is the number of moles of electrons involved, E_{r} is the reversible potential, and F is Faraday's constant. In the zinc–air systems, $E_{\text{r}} = 1.65$ V.

At the end, the residual particles were analyzed by means of the scanning electron microscope to compare their surface aspect before and after the discharging process. Moreover, an electrochemical impedance spectroscopy (EIS) has been done, since this experimental procedure, encompassing a sufficiently broad range of frequencies, allowed to isolate and distinguish the influence of the governing physical and chemical phenomena at a given applied potential.[43,44] The data obtained from the EIS analysis have been represented by the Nyquist plot.

In order to make an easier interpretation of the results of the present work, it seems appropriate to summarize some elements of electrochemistry, because the characterization of an electrochemical system with EIS requires the interpretation of the data with the help of suitable models. These models consist of equivalent circuits which are built with the help of well-known passive electrical elements, such as resistors, capacitors, inductors, and distributed elements (e.g., constant phase element (CPE) and Warburg impedance); each electrical element of an equivalent circuit describes a phenomenon occurring inside the electrochemical system, such as the interface electrode–electrolyte or the ohmic resistance of the electrolyte.[44] Hence, these elements can be combined in series and parallel to give complex equivalent circuit which depend on shape and values of the Nyquist plot. For example, in **Figure 5** is reported the equivalent circuit model used to describe electrode processes when both kinetics and diffusion are non-negligible. It includes a solution resistance (R_{Ω}), a double layer capacitor C, or CPE, the charge transfer resistance (R_{ct}) and the so-called Warburg element, Z_{WAR}, which contains information on the diffusion coefficient of the species. Besides, in Figure 5 (right) is also reported a Nyquist plot from which the equivalent circuit could be derived.[45]

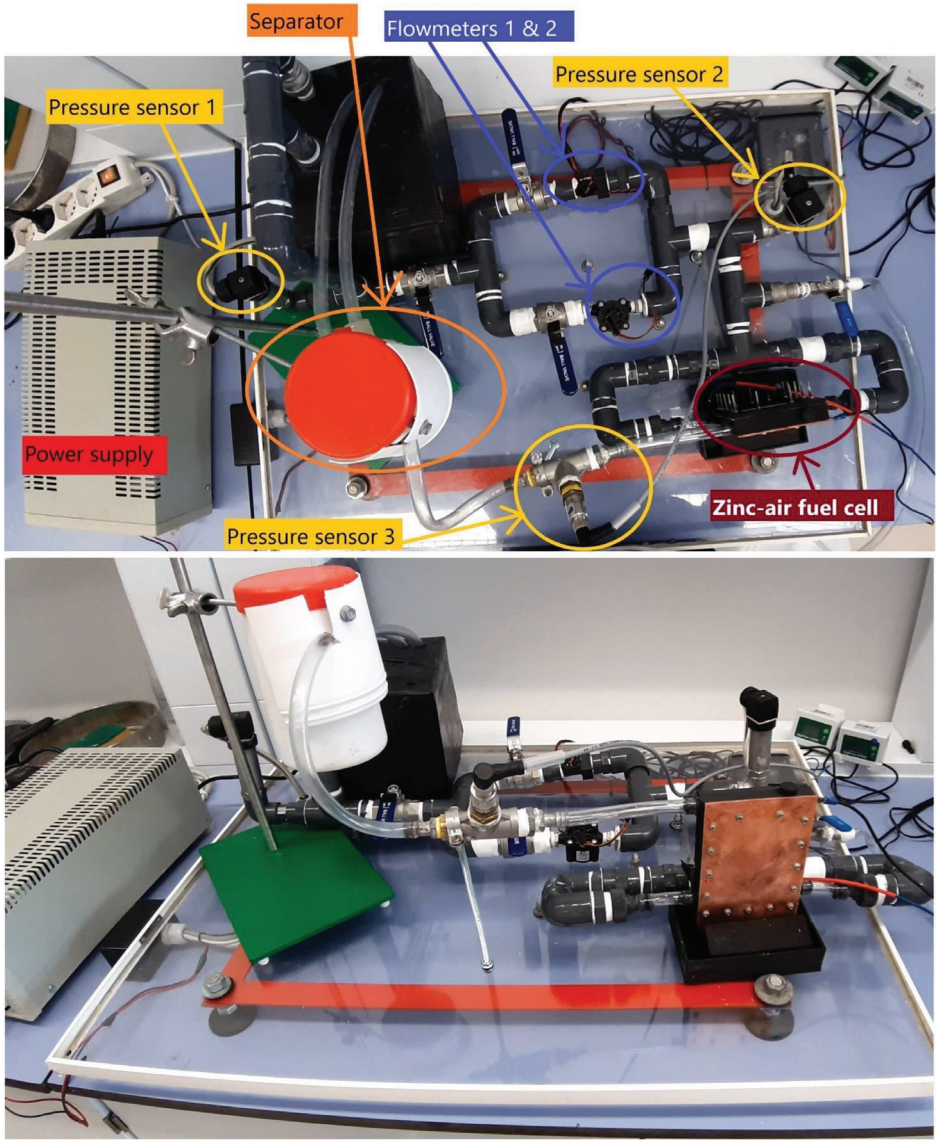

Figure 4. Images of the entire experimental setup.

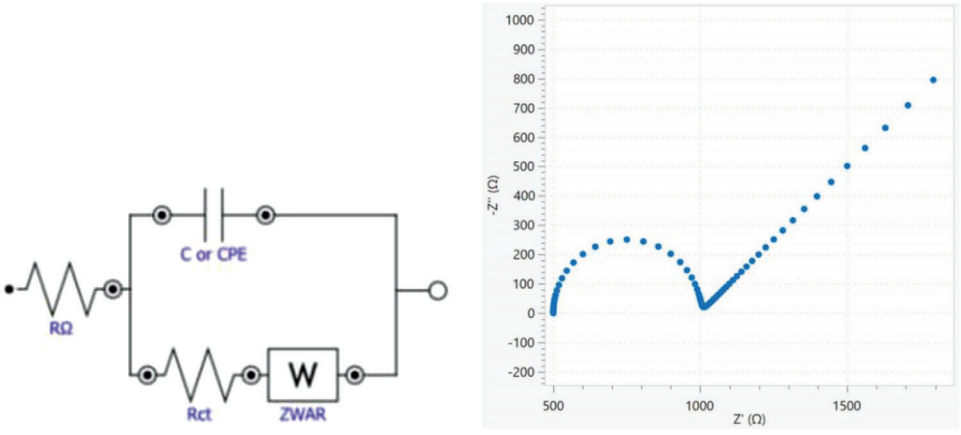

Figure 5. Left): Equivalent circuit model for kinetic and diffusion control used to characterize a ZAFC. Right): A typical Nyquist plot resulting from the equivalent circuit.

In the case of Figure 5, the equivalent circuit of the ZAFC is composed by

- two resistance elements, which represent the main electrochemical phenomena within the ZAFC; particularly, the resistors are the ohmic resistance of the electrolyte (R_Ω) and the polarization resistance (R_{ct}) related to the polarization of an electrode when its potential is forced away from its value at open circuit due to the current flow.

The values of R_Ω and R_{ct} could be calculated directly from the Nyquist plot because they correspond to the intersection points of the Nyquist plot with the x-axis.

- a capacitance element (C or CPE), which describes the interface electrode/electrolyte, where there is a double electrical layer. This double layer is formed as ions from the solution approach the electrode surface. The charges in the electrode are separated from the charges of these ions and the separation is of the order of Angstroms. The value of the double layer capacitance depends on many variables including electrode potential, temperature, ionic concentrations, types of ions, oxide layers, electrode roughness, impurity adsorption, etc.

The CPE is often used instead of a capacitor in order to model, for example, the nonideality of the electrode surface or of a coating layer (roughness).

When the capacitance (or the constant phase element) is in parallel with a resistor, its value can be determined through visual observation method. In this case, C is in parallel with R_{ct} and both are in series with R_Ω.

The linear frequency (ω) at which the top of the semicircle occurs, ν_{top}, is related to the capacitance value C, then the C value can be calculated by the following equation[45]

$$C(\omega) = \frac{1}{2\pi R_{ct} \nu_{top}} \tag{8}$$

The Warburg impedance (W) was introduced to model the diffusion of ionic species through the diffusion boundary layer. The impedance of a Warburg element Z_W is shown in the following equation[45]

$$Z_W = \frac{1}{Y_0 \sqrt{j\omega}} \tag{9}$$

Where $j = \sqrt{-1}$, ω is the frequency, and Y_0 is a parameter containing information on the diffusion of ionic species through the diffusion boundary layer. A suitable value for Y_0 can be calculated by performing a linear regression on the linear section of the Nyquist diagram: the Y_0 value is calculated as the reciprocal of the intercept value of the line on which the straight section of the Nyquist diagram lies on the x-axis[45]

$$Y_0 = \frac{1}{x} \tag{10}$$

Where x is the intercept value of the line on which the straight section of the Nyquist diagram lies on the x-axis.

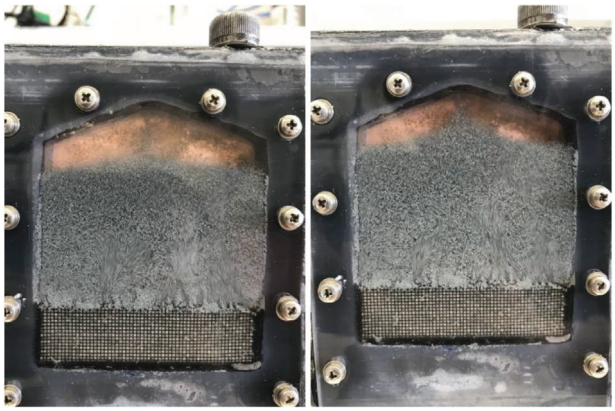

Figure 6. Example of operating fluid bed.

3. Discussion of Results

The fluidized bed has been characterized by measuring height of the bed, flow rate of electrolyte, and pressures in different points of the setup. **Figure 6** shows an image related to the fluid bed in operation. Between the inlet channels and the bottom of the fluid bed, can be seen the distributor, consisting of a compact bed of zirconia spheres, that has been used to improve the homogenization of the flow, which is fully developed without the formation of preferential pathways.

The main results related to the fluid-dynamic characterization of the zinc particle bed are summarized in **Figure 7**.

From this experimental characterization, it is possible to observe that the bed height without electrolyte flow is equal to 1.5 cm. Therefore, low flowrate values (up to 1.5 L min^{-1}) produce a growth of the bed height characterized by a constant slope (blue line in the left side of the graph): in this phase, the bed is not moving and can be defined fixed. Over 1.8 L min^{-1} the bed is completely fluidized, while in the range from 1.5 to 1.8 L min^{-1} there is a transition zone where the particles of different size start to fluidize, from the smallest to the biggest.

The slope of the bed height curve is higher in the fluidized bed condition compared to the fixed bed one because the particles became freer to move, hence the fluidized bed required less increase in flow to expand than the fixed bed.

The pressure curve (red line) presents the same transition behavior in the same flow rate range. Furthermore, the slope of the pressure curve in the fluidized bed condition is lower than the fixed bed condition. The cause of this behavior is the same of the bed height, therefore the particles being freer to move produce a lower pressure gradient to increase the bed height.

Once the correlation between flow rate and bed height has been characterized, these results were used to obtain, and then to compare, the polarization curves of the ZAFC in different flow-dynamic conditions in order to know how these parameters can influence the performance of the cell. **Figure 8** shows the most significant polarization curves obtained with different bed height.

The slope of the linear part of the I–V plot gives information about the ohmic resistance of the electrochemical cell, which is related to the conductance of the electrolyte and to the contact between zinc particles each other. As it can be seen, with a fixed

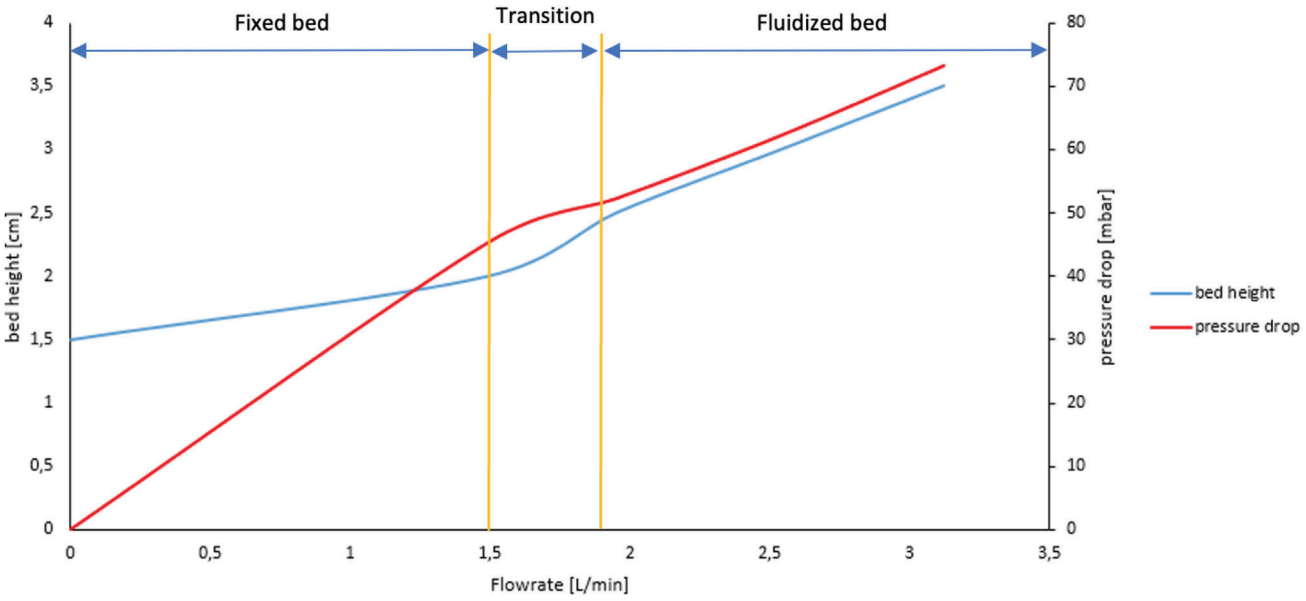

Figure 7. Fluid-dynamic characterization of the zinc particle bed. Blue line represents the values of the bed height as a function of the flowrate. Red line represents the values of the pressure drop as a function of the flowrate.

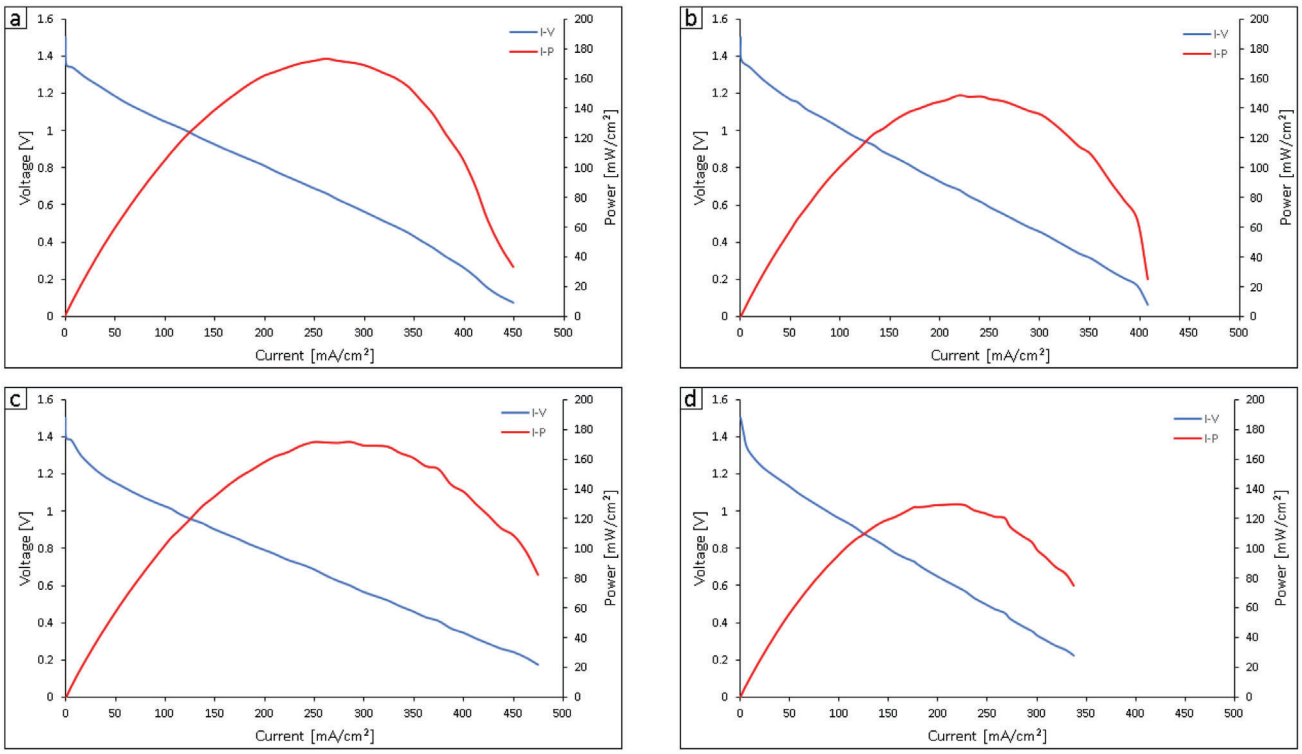

Figure 8. Polarization curves in different conditions of the bed: a) fixed expanded bed. b) Transition conditions from fixed bed to fluidized bed. c) Fluidized bed with a bed height of 2.5 cm. d) Fluidized bed with a bed height of 3.0 cm.

bed of zinc particles (Figure 8a) the cell produced, at the maximum power point (MPP), a peak power of 173 mW cm^{-2} corresponding to a current value of 262 mA cm^{-2} and a voltage of 0.67 V, while the maximum delivered current was 449 A cm^{-2} with an ohmic resistance of about 0.190 Ω. In the transition condition (from fixed bed to fluidized bed- Figure 8b) the ZAFC produced, at the MPP, a peak power of 149 mW cm^{-2} corresponding to a current value of 219 mA cm^{-2} and a voltage of 0.68 V, while the maximum delivered current was 408 mA cm^{-2} with an ohmic resistance of about 0.209 Ω. In the case of fluidized bed

Table 1. Performance comparison with other research groups which used manganese-based catalyst for ORR.

Research group	Anode	MPP [mW cm^{-2}]	Current density at MPP [mA cm^{-2}]	Potential at MPP [V]	Maximum current density delivered [mA cm^{-2}]
This study	Zinc powder	173	262	0.67	449
Pei et al.[10]	Zinc pellet	435[a)]	510[a)]	0.86[a)]	570[a)]
Ma et al.[14]	Zinc plate	60.4	80	≈0.7/0.8	150
Lee et al.[11]	Zinc powder	120	≈175	≈0.7	200
Sumboja et al.[12]	Zinc plate	108	168	≈0.6	170
Chen et al.[23]	Zinc powder	427.7[b)]	518.6[b)]	0.8[b)]	≈660[b)]

[a)] Differently from this study, the air was fed in the air-cathode by a fan; [b)] Differently from this study, the air-cathode was feed with oxygen (not with air).

with a bed height of 2.5 cm (Figure 8c) the cell produced, at the MPP, a peak power of 171 mW cm^{-2} corresponding to a current value of 286 mA cm^{-2} and a voltage of 0.62 V, while the maximum delivered current was 475 mA cm^{-2} with an ohmic resistance of about 0.175 Ω. Finally, with a condition of fluidized bed with a bed height of 3.0 cm (Figure 8d) the cell produced, at the MPP, a peak power of 129 mW cm^{-2} corresponding to a current value of 207 mA cm^{-2}, a voltage of 0.60 V, a maximum delivered current of 337 mA cm^{-2} and an ohmic resistance of about 0.232 Ω.

Comparing the different polarization curves, it can be concluded that the condition of fluidized bed did not lead to improved performance against the condition of fixed bed; this is reasonable because the reaction conditions, such as amount of zinc powder and concentration of electrolyte, were always the same.

However, it could be observed a little difference in slope of the linear part of the *I–V* plot: the highest ohmic resistance was observed in transition condition, when also the specific performance of the ZAFC resulted lower than in the other cases (due to the bigger height of fluidized bed). These results can be explained by taking into account the contact between the particles, which in these conditions moved in an irregular mode, reducing the probability to have contact between particles. The lowest ohmic resistance was observed in the fluidized bed conditions with a bed height of 2.5 cm (0.175 Ω), while, in the fixed bed was observed an ohmic resistance value of 0.190 Ω which is little higher than that in the fluidized bed condition.

In order to compare the performance of the present work with that published in previous articles, **Table 1** summarizes the best ZAFC performance obtained in recent years by research groups which worked with manganese-based catalyst for the ORR reaction.

As it can be seen, the highest performances have been obtained by using zinc powder/pellet: this suggests that the use of zinc particles provides a greater active surface area than other configurations, improving the reactions between zincate and OH^-. Moreover, Pei et al.[10] and Chen et al.[23] obtained very high performance, also compared with that of this study, but they developed their experiments, exploiting the positive effect of a higher partial pressure of the oxygen on the air-cathode, obtained by using an electric fan and pure oxygen, respectively.

Once the characterization of the cell performance with different flow rates of electrolyte was done, it was carried out the endurance test of the ZAFC by applying a constant current load and then monitoring the potential difference at the terminals of the cell and its power output. This test was carried out in two different fluid dynamic conditions: fixed bed and fluidized bed with a bed height of 2.5 cm (**Figure 9**).

This analysis highlighted that, in the first 50 min of operation, the performance in the two conditions was the same and then the fluidized bed conditions enhance better performance up to about 320 min of operation. At the same time, the different hydrodynamic conditions produced diverse pressure drop through the hydraulic circuit and therefore diverse electrical power values absorbed by the pump, respectively, 0.4 W in the fluidized bed conditions and 0.18 W in the fixed bed conditions.

After these 320 min of operation, the cell with fluidized bed conditions discharged abruptly, while the cell with fixed bed conditions continued to generate energy for about 150 min but with low power.

The rapid discharge of the fluidized bed cell after 320 min of operation was because, due to the increased flow of electrolyte, zinc particles were carried away and not replenished; while in the fixed bed conditions the particles were carried out more slowly hence the residual particles continued to generate energy with lower power.

In the curve for fluidized bed conditions, it can also be seen that there is a positive step up in cell performance after about 220 min. This behavior has been observed repetitively in all endurance tests, that have been performed under fluidized bed conditions: the reason for this behavior is currently unclear and therefore needs further study and investigation.

It can be also observed that the fixed bed curve (blue line) is more regular than the fluidized bed one (red line): this behavior can be explained taking into account that the ohmic resistance of the cell is also related to the contact between zinc particles, which is unstable in the fluidized bed condition, where the particles are constantly moving and are not in constant and regular contact each other, leading to a little variation of the instantaneous ohmic resistance.

Another endurance analysis was conducted to compare the performance of the cell applying different current loads in the same fluid dynamic conditions (**Figures 10** and **11**). Particularly, three constant current loads of 175, 225 and 250 mA cm^{-2} were applied to the ZAFC; these values were chosen from the polarization curve: 250 mA cm^{-2} corresponds to the MPP, 175 mA cm^{-2} is the value in which the slope of the polarization curve starts to

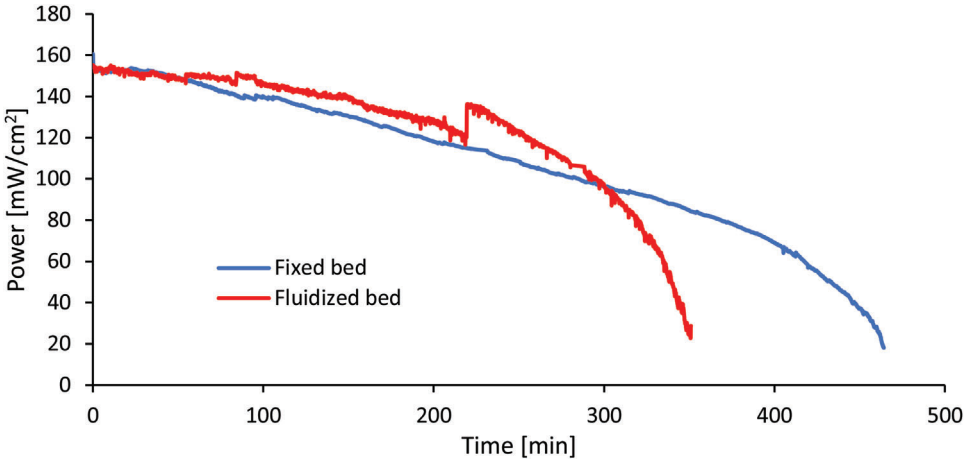

Figure 9. Endurance test comparison in fixed bed (blue curve) and fluidized bed (red curve) conditions.

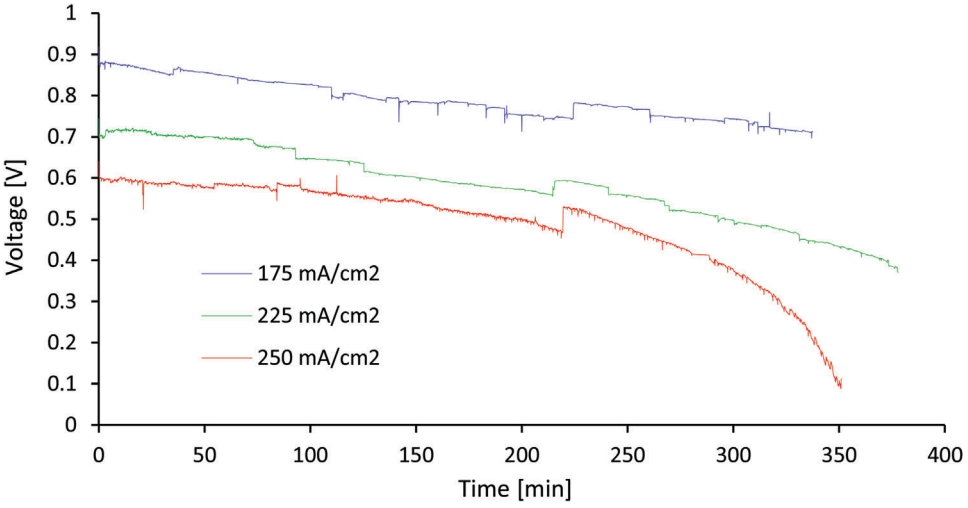

Figure 10. Cell voltage during the discharge process. Blue line corresponds to a constant current load of 175 mA cm^{-2}; green line corresponds to a constant current load of 225 mA cm^{-2}; red line corresponds to a constant current load of 250 mA cm^{-2}.

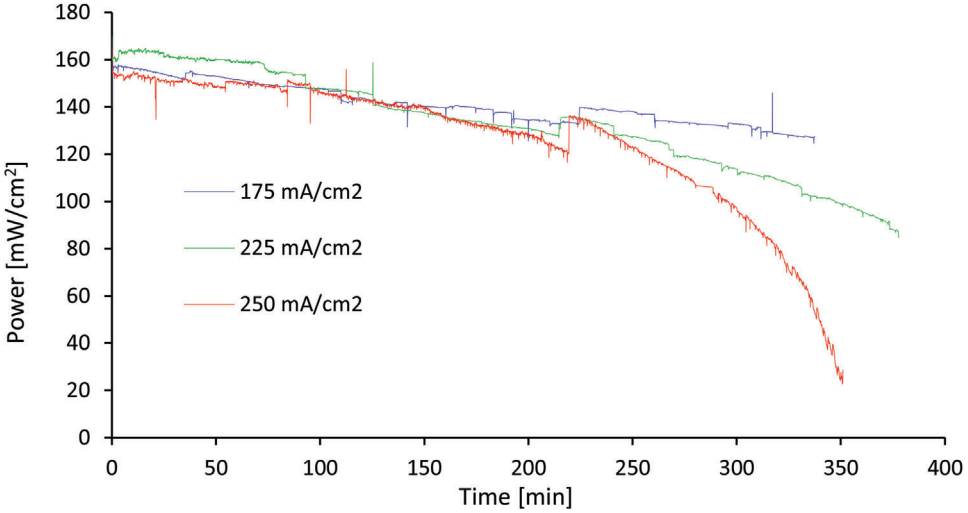

Figure 11. Power production during discharge process. Blue line corresponds to a constant current load of 175 mA cm^{-2}; green line corresponds to a constant current load of 225 mA cm^{-2}; red line corresponds to a constant current load of 250 mA cm^{-2}; all lines have been measured in fluidized bed conditions, with a flowrate of 2.0 l min^{-1}.

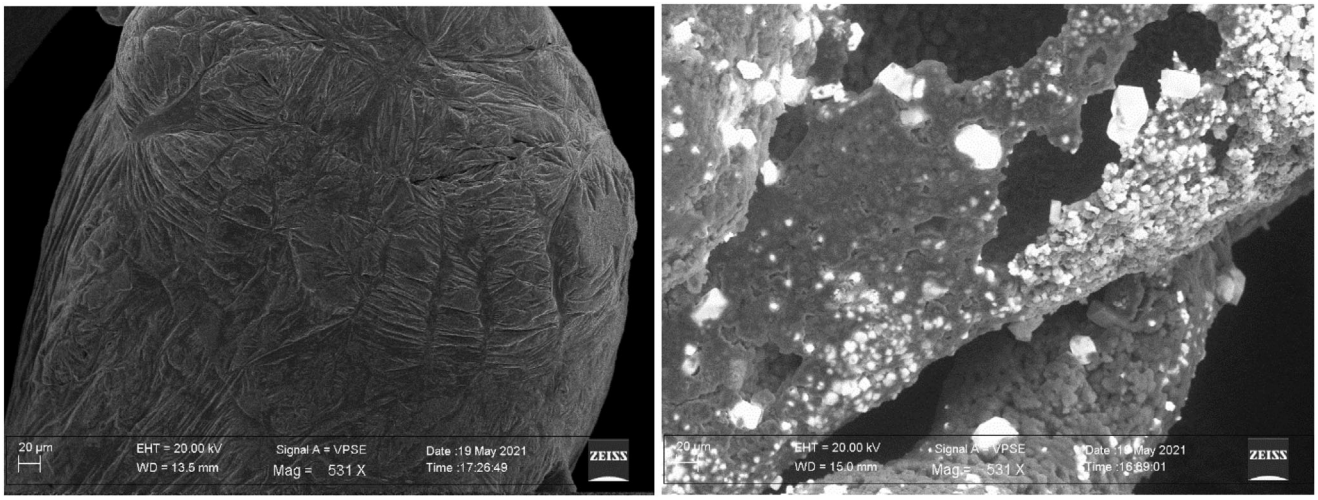

Figure 12. SEM images of the surface of the zinc particles before the discharging process (on the left) and after the discharging process (on the right).

decrease and finally the value of 225 mA cm^{-2} is an intermediate value between the previous ones.

In each of these three cases, the performance worsened with time. The power production in the three tests was the same up to 250 min of operation, after this time the cell in the test with higher current load rapidly discharged because zinc particles were carried away and not replenished while in the other cases the particles were not yet small enough to cause particle transport away from the cell. Therefore, the higher is the applied current load, the faster is the consumption of zinc particles and the performance started to drop down quickly when the particle size was small enough to cause particle transport away from the cell.

However, it is important to note that although the three power curves are initially comparable, the related energy conversion efficiencies are different. Indeed, the voltage-time curves suggest that the efficiency is much lower in the case with a constant current load of 250 mA cm^{-2} than in the case with a constant current load of 175 mA cm^{-2}. More in details, the average energy conversion efficiency (calculated with the Equation (7) in which W_{el} was measured experimentally) in the test with a constant current load of 175 mA cm^{-2} was about 46%, while the average energy conversion efficiency in the test with a constant current load of 250 mA cm^{-2} was about 29%. These values would be significantly higher if the electrolyte was freshly reinserted every 150 min of operation; indeed, the average energy conversion efficiency of the first 150 min of operation in the test with a constant current load of 175 mA cm^{-2} was about 51%, while for the test with a constant current load of 250 mA cm^{-2} it was about 35%.

Below are reported the images obtained from the SEM analysis of the zinc particles before and after the discharging process (**Figure 12**). As it can be seen from the SEM images, before the discharging process the zinc surface appears uniform, compact, and relatively smooth. While, at the end of the discharging process, the zinc particles appear irregular with zinc oxide deposits covering almost the entire surface.

Zinc oxide deposits are one of the main causes of progressive reduction in performance, since zinc oxide hinders the oxidation of zinc atoms both as an insulator and as a reaction product. The formation of the zinc oxide layer is due to the local attainment of saturation conditions of the electrolyte (saturation relative to the concentration of $Zn(OH)_4^{2-}$). In the proximity of the surface of the zinc particles, where the oxidation reaction of the zinc atoms takes place, there is a higher concentration of $Zn(OH)_4^{2-}$ than at other points in the entire system. Therefore, when the average concentration of $Zn(OH)_4^{2-}$ in the electrolyte is very low, even in the proximity of the particles saturation conditions are not reached; however, as the average concentration of $Zn(OH)_4^{2-}$ in the electrolyte increases, the probability of reaching saturation conditions near the surface of the zinc particles increases. As seen above, reaching saturation conditions of $Zn(OH)_4^{2-}$ in the electrolyte leads to the formation of ZnO which is not soluble and precipitates as an electrically insulating solid. As the saturation conditions are reached locally in the proximity of the zinc particles, the ZnO formed is deposited on their surface, forming an insulating layer that hinders the oxidation of the zinc atoms below it.

Finally, **Figure 13** shows the results obtained by the EIS analysis performed in fluidized bed conditions and the corresponding equivalent circuit.

From the Nyquist diagram of Figure 13 and by means of the above-described mathematical model, the following values were obtained for the equivalent circuit describing the analyzed ZAFC: $R_\Omega = 0.0203\ \Omega$, $R_{ct} = 0.067\ \Omega$, $Y_0 = 16.31\ S \cdot s^{0,5}$, and $C = 0.0144$ F. The comparison between the Nyquist of Figure 13 and the Nyquist related to a ZAFC based on zinc plate as anode,[33] allows to conclude

(a) the ohmic resistances related to the electrolyte ionic conductivity R_Ω have the expected value of about 0.02 Ω, because the two fuel cells are based on the same electrolyte;

(b) the impedance related to the charge transfer resistance R_{ct} has a lower value due to impact of the particles each other which lead to breaking the passivation layer from the zinc particles surface;

(c) the capacitance used to describe the interface electrode/electrolyte C, instead, is little higher than that

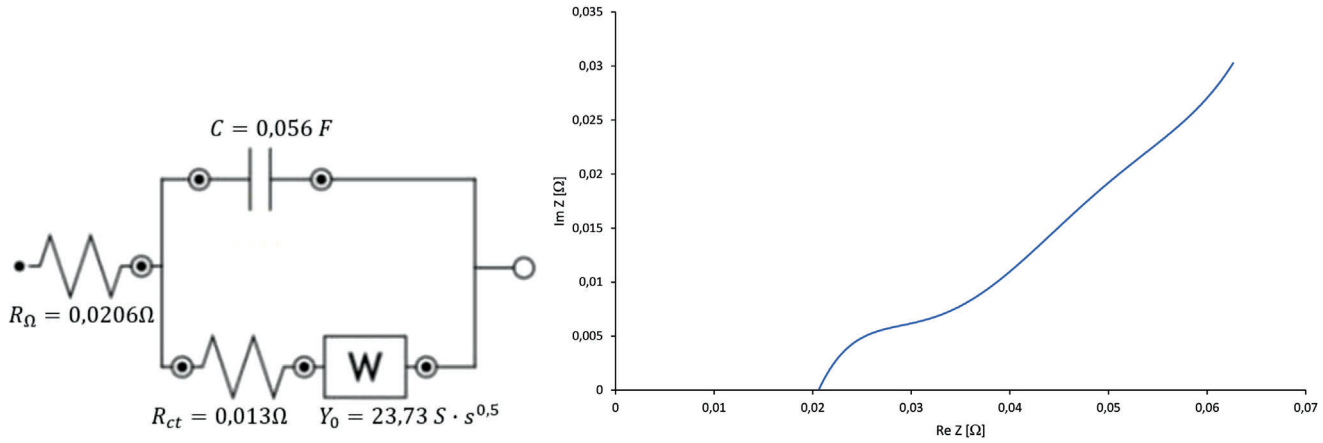

Figure 13. Nyquist plot and equivalent circuit model obtained by the EIS analysis.

obtained by the Nyquist plot of Pei et al.,[33] due to the higher surface of zinc particles which lead to a higher interface electrode/electrolyte, hence, to a higher equivalent capacitance C;

(d) finally, the value of parameter Y_0, which is related to the diffusion of ionic species through the diffusion boundary layer, is very similar because in both works a flowing electrolyte was used, which homogenized the distribution of ionic species produced at the electrodes, thereby reducing the thickness of the diffusion boundary layer.

4. Conclusions and Outlook

In the present work, a novel fluidized-bed ZAFC has been designed, built, tested, and characterized. The main results can be summarized as in the following

- The electrolyte flow rate does not positively influence the performance of the ZAFC. Therefore, seeing the bed height behavior shown in Figure 7 and the ZAFC polarization curves shown in Figure 8 it can be suggested that the electrochemical performance are slightly lower in the transition conditions of the bed from fixed to fluidized bed and in the high fluidized bed conditions, in comparison with the performance of the cell in the condition of fixed bed and low fluidized bed. The explanation of this behavior could be found in the different condition of contact between zinc particles inside the cell.
- The ohmic resistance of the cell is slightly lower in the fluidized bed conditions than in the fixed bed conditions.
- In the fluidized bed conditions, particles are moved out of the cell when they become enough small to be transported from the electrolyte flux. This is important to replace spent zinc particles with new ones, in order to obtain constant high performance.
- The performance of the ZAFC declines during operating time, because the electrolyte reaches the saturation condition in proximity of zinc particles.
- The SEM analysis, which has been done before and after the discharge process evidenced solid, porous, nonconductive layers of zinc oxide on zinc particle surface.
- The EIS analysis has evidenced the importance of the fluidized bed to reduce the electrochemical losses; even if the high surface of zinc particle causes a high value of the capacitance, which describes the interface electrode/electrolyte.

To further improve the performance of novel fluidized-bed ZAFC, it will be important to develop a model able to optimize the amount of zinc powder inside the cell and the electrolyte working time. This can be obtained by coupling mathematical/theoretical knowledges with experimental results.

Besides, it will be needed to make several experimental tests to develop a further model able to predict the performance of the cell in different operation conditions: this model will be very important in the development of management systems for electrochemical devices, which have to be implemented in industrial plants.

Finally, taking into account the results of the present study, it can be concluded that the coupling of zinc particles with a flowing electrolyte can lead to very promising way for high performance ZAFC development.

Conflict of Interest

The authors declare no conflict of interest.

Data Availability Statement

The data that support the findings of this study are available from the corresponding author upon reasonable request.

Keywords

energy storages, flowing electrolytes, fluidized beds, zinc particles, zinc–air fuel cells

Received: March 13, 2023
Revised: June 8, 2023
Published online: July 6, 2023

[1] H. Hassanzadeh, S. H. Mansouri, *Proc. Inst Mech. Eng., Part A* **2005**, *219*, 245.

[2] H. Nourianfar, H. Abdi, *Sustainable Energy, Grids Networks* **2021**, *26*, 100449.
[3] C. Kim, *Renewable Sustainable Energy Rev.* **2021**, *144*, 110870.
[4] I. Hadjipaschalis, A. Poullikkas, V. Efthimiou, *Renewable Sustainable Energy Rev.* **2009**, *13*, 1513.
[5] C. K. Das, O. Bass, G. Kothapalli, T. S. Mahmoud, D. Habibi, *Renewable Sustainable Energy Rev.* **2018**, *91*, 1205.
[6] M. Xu, D. G. Ivey, Z. Xie, W. Qu, *J. Power Sources* **2015**, *283*, 358.
[7] M. R. von Spakovsky, B. Olsommer, *Energy Convers. Manage.* **2002**, *43*, 1249.
[8] P. Pei, K. Wang, Z. Ma, *Appl. Energy* **2014**, *128*, 315.
[9] O. Z. Sharaf, M. F. Orhan, *Renewable Sustainable Energy Rev.* **2014**, *32*, 810.
[10] P. Pei, Z. Ma, K. Wang, X. Wang, M. Song, H. Xu, *J. Power Sources* **2014**, *249*, 13.
[11] J. S. Lee, T. Lee, H. K. Song, J. Cho, B. S. Kim, *Energy Environ. Sci.* **2011**, *4*, 4148.
[12] A. Sumboja, X. Ge, F. W. T. Goh, B. Li, D. Geng, T. S. A. Hor, Y. Zong, Z. Liu, *ChemPlusChem* **2015**, *80*, 1341.
[13] P. Sapkota, H. Kim, *J. Ind. Eng. Chem.* **2010**, *16*, 39.
[14] H. Ma, B. Wang, Y. Fan, W. Hong, *Energies* **2014**, *7*, 6549.
[15] J. S. Lee, G. S. Park, H. I. Lee, S. T. Kim, R. Cao, M. Liu, J. Cho, *Nano Lett.* **2011**, *11*, 5362.
[16] Y. Li, M. Gong, Y. Liang, J. Feng, J. E. Kim, H. Wang, G. Hong, B. Zhang, H. Dai, *Nat. Commun.* **2013**, *4*, 1805.
[17] Y. Meng, Y. M. Zhao, J. C. Li, C. Shi, L. Zhang, P. X. Hou, C. Liu, H. M. Cheng, *NPG Asia Mater.* **2023**, *15*, 14.
[18] S. Zhu, Z. Chen, B. Li, D. Higgins, H. Wang, H. Li, Z. Chen, *Electrochim. Acta* **2011**, *56*, 5080.
[19] Q. Liu, Y. Wang, L. Dai, J. Yao, *Adv. Mater.* **2016**, *28*, 3000.
[20] Y. Li, H. Dai, *Chem. Soc. Rev.* **2014**, *43*, 5257.
[21] S. I. Smedley, X. G. Zhang, *J. Power Sources* **2007**, *165*, 897.
[22] J. Fu, Z. P. Cano, M. G. Park, A. Yu, M. Fowler, Z. Chen, *Adv. Mater.* **2017**, *29*, 1604685.
[23] P. T. Chen, T. Sangeetha, T. W. Hsu, C. J. Yang, T. Y. Yung, W. M. Yan, K. D. Huang, *Chem. Phys. Lett.* **2019**, *728*, 160.
[24] J. S. Lee, S. T. Kim, R. Cao, N. S. Choi, M. Liu, K. T. Lee, J. Cho, *Adv. Energy Mater.* **2011**, *1*, 34.
[25] S. B. Sherman, Z. P. Cano, M. Fowler, Z. Chen, *AIMS Energy* **2018**, *6*, 121.
[26] M. A. Rahman, X. Wang, C. Wen, *J. Electrochem. Soc.* **2013**, *160*, A1759.
[27] C. W. Lee, S. W. Eom, K. Sathiyanarayanan, M. S. Yun, *Electrochim. Acta* **2006**, *52*, 1588.
[28] P. Sapkota, H. Kim, *J. Ind. Eng. Chem.* **2009**, *15*, 445.
[29] A. R. Mainar, E. Iruin, L. C. Colmenares, A. Kvasha, I. de Meatza, M. Bengoechea, O. Leonet, I. Boyano, Z. Zhang, J. A. Blazquez, *J. Energy Storage* **2018**, *15*, 304.
[30] J. Cooper, US Patent 5 434,020 **1995**.
[31] J. J. Han, N. Li, T. Y. Zhang, *J. Power Sources* **2009**, *193*, 885.
[32] T. Sangeetha, P. T. Chen, W. F. Cheng, W. M. Yan, K. D. Huang, *Energies* **2019**, *12*, 1090.
[33] P. Pei, S. Huang, D. Chen, Y. Li, Z. Wu, P. Ren, K. Wang, X. Jia, *Appl. Energy* **2019**, *241*, 124.
[34] X. Zeng, J. Hao, Z. Wang, J. Mao, Z. Guo, *Energy Storage Mater.* **2019**, *20*, 410.
[35] V. Neburchilov, H. Wang, J. J. Martin, W. Qu, *J. Power Sources* **2010**, *195*, 1271.
[36] F. Bidault, D. J. L. Brett, P. H. Middleton, N. Abson, N. P. Brandon, *Int. J. Hydrogen Energy* **2010**, *35*, 1783.
[37] G. Li, M. A. Mezaal, R. Zhang, K. Zhang, L. Lei, *Fuel Cells* **2016**, *16*, 395.
[38] Y. Gorlin, T. F. Jaramillo, *J. Am. Chem. Soc.* **2010**, *132*, 13612.
[39] A. R. Mainar, O. Leonet, M. Bengoechea, I. Boyano, I. de Meatza, A. Kvasha, A. Guerfi, J. A. Blázquez, *Int. J. Energy Res.* **2016**, *40*, 1032.
[40] C. J. Yang, P. T. Chen, K. D. Huang, *Int. J. Energy Res.* **2020**, *44*, 4224.
[41] S. Thomas, I. S. Cole, M. Sridhar, N. Birbilis, *Electrochim. Acta* **2019**, *97*, 192.
[42] V. S. Bagotsky, *Foundamentals of Electrochemistry*, Wiley-Interscience, Moscow **2006**.
[43] S. Srinivasan, *Fuel Cells From Fundamentals to Applications*, Springer, New York **2006**.
[44] R. M. Evgenij Barsoukov, *Impedance Spectroscopy Theory, Experiment, and Applications*, John Wiley & Sons, Hoboken, NJ **2005**.
[45] M. Autolab, EIS Data fitting – How to obtain good starting values of equivalent circuit elements https://www.metrohm.com (accessed: May 2019).